Optical Properties of ZnO Nanowires and Nanorods Synthesized by Two Step Oxidation Process

V. Ghafouri [1], M. Shariati [1], A. Ebrahimzad[1]

Abstract

ZnO nanowires with a diameter of 70 nm and nanorods with a diameter in the range of 100-150 nm and two micrometer in length were grown on glass substrates by resistive evaporation method and applying a two-step oxidation process at low temperatures, without using any catalyst, template or buffer layer. The XRD pattern of these nanostructures indicated a good crystallinity property with wurtzite hexagonal structure. Photoluminescence measurement revealed three band emissions; one sharp strong peak in the UV region and two weaker peaks in the visible region, indicate good optical properties of nanorods synthesized by this method. Heat treatment in oxygen-rich atmosphere results to decrease of deep-level emission intensity in the PL spectra. The relatively high intensity of UV emission implies that this approach is a simple and promising method for fabricating ZnO nanorods in order to be used in optoelectronic devices especially in the UV range of the spectrum.

Keywords: ZnO Nanowires; Nanorod; Resistive Evaporation; Oxidation; Photoluminescence

1. Introduction

Zinc oxide (ZnO) is a direct band gap semiconductor from the II-VI group with a wide band gap of 3.37 eV. It has a large exciton binding energy of 60 meV. It is an increasingly important photonic material and is considered to be one of the most significant semiconductor materials for application in optoelectronics, sensor, actuators and ferromagnetism due to its unique properties [1- 5].

Many research groups have developed various synthesis methods for growing 1D ZnO nanostructures such as whisker, nanowire, nanorod, nanonail, nanoring, etc. [6-11]. The synthesis process of 1D ZnO nanorods and nanowires has mainly been conducted via vapor-solid (VS) growth mechanism without metal catalyst or vapor-liquid-solid (VLS) mechanism using metal catalyst in which the catalyst form the liquid phase in the initial growth stage [7,12].

Although 1D ZnO nanostructures have been fabricated using different methods including thermal evaporation, chemical vapor deposition (CVD), metal organic chemical vapor deposition (MOCVD) and sol-gel process [12-15], there are still some drawbacks in applying these techniques in manufacturing ZnO nanostructures. In all these processes a relatively high growth temperature is required. As an example, for growing ZnO nanowires and nanorods a growth temperature of about 750-1300 °C should be provided [16, 17]. Moreover some of the equipments used in these processes are very expensive. Therefore there are still some limitations in commercial production of ZnO nanostructures.

Also, there are difficulties in making use of metal catalysts for synthesis of ZnO nanostructures. Most metal catalysts, such as Au and Ni, are impurities that generate an unintentional trap level in the band gap of semiconductors. These trap sites act as deep-level non-radiative recombination centers in optoelectronic materials which deteriorate emission efficiency.

During all these passed years less attention has been put into synthesis of Zn/ZnO nanowires and nanorods by using resistive evaporation technique and applying dry oxidation. In this research by using this simple and cheap method we fabricated Zn/ZnO nanowires and nanorods at low temperature without any catalyst, template or buffer layer. Photoluminescence measurement revealed three band emissions; one sharp

1- Research Institute of Applied Sciences (ACECR), Shahid Beheshti University, Tehran, Iran.

Corresponding author:
V. Ghafouri, Research Institute of Applied Sciences (ACECR), Shahid Beheshti University, Tehran, Iran.
Email: ghafori@rias.ac.ir

strong peak in the UV region and two weaker peaks in the visible region, indicate good optical properties of nanorods synthesized by this method. ZnO nanorods and nanowires synthesized by this method would be promising to applying ZnO nanostructures with good structural and optical properties to be used in UV optoelectronic devices.

2. Experimental

For growing ZnO nanowires and nanorods, firstly, a thin layer of metallic zinc was deposited on 7059 corning glass substrates by using resistive evaporation technology. Then the films were heat treated in a two-step oxidation process. Metallic zinc granules with a purity of 99.99% were used as the source material for deposition of Zn thin films and oxygen gas with a purity of 99.999% was used for oxidation process in this study, and tungsten boat was chosen as a resistively heated source for the evaporation.

The information about the deposition condition is given in Table 1 for all samples. Before the first oxidation step samples A, B and C were pre-annealed in vacuum condition in the deposition chamber for about thirty minutes. Just after pre-annealing in vacuum, the first oxidation step was carried out in the deposition chamber, in which oxygen gas was introduced into the chamber and the films were annealed in oxygen atmosphere at a relatively low temperature.

The details of this heat treatment are given in Table 2. A tube furnace was used for the second oxidation step in which there was a continuous flow of oxygen during annealing while the oxygen pressure was kept constant at 1 mbar for all samples. The data related to this process is given in table 3.

The crystalline structure of the products were characterized by X-ray diffraction method using CuKα radiation (λ=1.54 nm) with the scanning 2θ angle ranging from 20 to 80 degree. The morphology of synthesized nanostructures was studied by Hitachi S-4160 field emission scanning electron microscope and the PL spectra were obtained with an excitation wavelength of 300 nm of a Xe lamp.

3. Result and Discussion

Figure 1 shows the FESEM images of sample A before (a) and after (b) the first oxidation step. It can be seen from image (a) that before annealing in oxygen, the substrate is uniformly covered with zinc nanosequins of 24 nm thick. Image (b) shows the surface of the substrate after the first oxidation process in oxygen atmosphere. It is seen that the structure of the deposited layer was changed from Zn nanosequins into ZnO nanowires that

Table 1. Deposition and first step oxidation process data into vacuum chamber

Parameter	Sample A	Sample B	Sample C	Sample D
Boat to substrate distance (cm)	19.0	11.0	9.0	6.0
Pre-deposition pressure (mbar)	2×10^{-5}	2×10^{-5}	1×10^{-2}	1×10^{-2}
Heating after deposition (°C)	161	122	90	-

Table 2. First step oxidation and annealing process data in vacuum chamber

Parameter	Sample A	Sample B	Sample C	Sample D
Oxygen gas pressure after deposition (mbar)	20	100	100	20
Final temperatur of heating into vacuum chamber (°C)	240	540	240	540
Time of heating into vacuum chamber (min)	60	120	30	90

Table 3. Second step oxidation and annealing process data in tube furnace

Parameter	Sample B	Sample C	Sample D
Pre-annealing pressure of tube furnace (mbar)	4×10^{-4}	4×10^{-4}	4×10^{-4}
Rate of oxygen flow into tube furnace (lit/min)	0.2	0.1	0.2
Annealing temperature into tube furnace (°C)	500	500	500
Time of annealing into tube furnace (min)	60	60	120
Ramping Rate of tube furnace (°C/min)	20	20	20

have an average diameter of 70 nm and a length of about 2 μm.

The nanosequins, in presence of oxygen gas, have acted as the source material for growing ZnO nanostructures and have been gradually transformed into nanowires. Figure 2(a) shows the nanosequins on the surface of sample C after the vacuum heat treatment. Figure 2(b) indicates the FESEM image of sample C after the second annealing in the stream of oxygen gas. In comparison with sample A, it can be seen that the structures in sample C tended to grow in the form of nanorods rather than nanowires, which is supposed to be the result of the second oxidation process in oxygen gas flow. The partially grown nanorods have a length of not more than 1μm and their diameter ranges between 100 to 150 nm. Figure 3 illustrates the XRD pattern of sample C. It is clear from the image that the Zn layer has not been oxidized completely, so both Zn and ZnO peaks can be seen in the X-ray pattern.

Figure 4(a) indicates the surface image of sample B before the first oxidation step, which is very similar to the morphology of sample A and C before the first oxidation. After comparing with sample D, which was not heat treated in vacuum, it was seen that

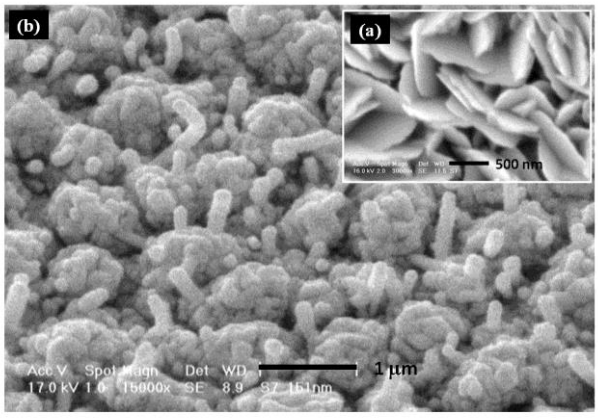

Fig 2. FESEM images of sample C. (a) indicates the nanosequins on the surface of sample C after the vacuum heat treatment and (b) indicates the FESEM image after the second annealing in the stream of oxygen gas. Scale bars for (a) and (b) images are 500 nm and 1 μm, respectively.

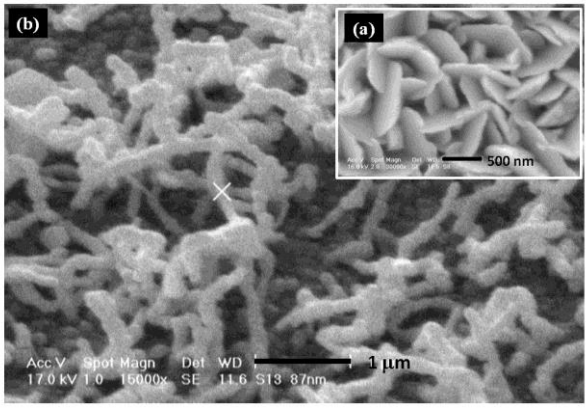

Fig. 1. FESEM images of sample A before (a) and after (b) the first oxidation step. Scale bars for (a) and (b) images are 500 nm and 1 μm, respectively.

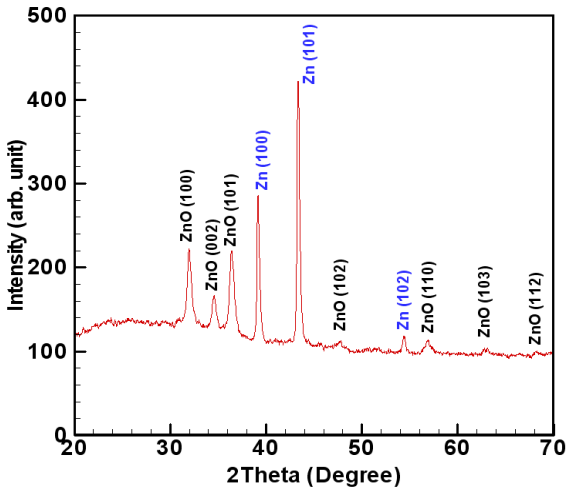

Fig. 3. The XRD pattern of sample C.

this similarity is the result of the annealing in vacuum condition before the first oxidation process. Figure 4 (b) shows the surface image of sample B after the second annealing process in oxygen flow. It is clear that, as in sample C, the second heat treatment has caused the structures to grow in a completely nanorod shape and in a direction almost vertical to the surface. The diameter of the nanorods in this sample varies in the range of 100-150 nm. The TEM image of a single nanorod of sample B is illustrated in figure 4(c). As it is seen in this image the diameter of this nanorod is about 60 nm and its length is less than 500 nm.

By comparing the surface morphology of sample C with the surface morphology of sample B it can be realized that the nanorods in sample B are shaped more completely and have grown with a preferential vertical orientation than in sample C. The only difference in the second oxidation step of these two samples was the flow of oxygen gas, which for sample B was twice the sample C, but in the first oxidation step there was a huge difference between the annealing temperatures. The annealing temperature of the first oxidation step was 240 and 540 °C for sample C and B, respectively. The first oxidation step was the time that Zn atoms interacted with oxygen molecules, and probably, it was in this stage that nucleation of the ZnO nanostructures took place. Thus, because of the higher temperature of sample B in this stage the nuclei were formed in sites that were more appropriate and shaped more completely in the form of ZnO nanostructures, but the complete growth of nanorods did not happen until after the second oxidation step that the initially shaped nanorods exposed to the flow of oxygen gas in a temperature of 500 °C. Figure 5 is the XRD pattern of sample B. All diffraction peaks match with the standard data of hexagonal structure of ZnO.

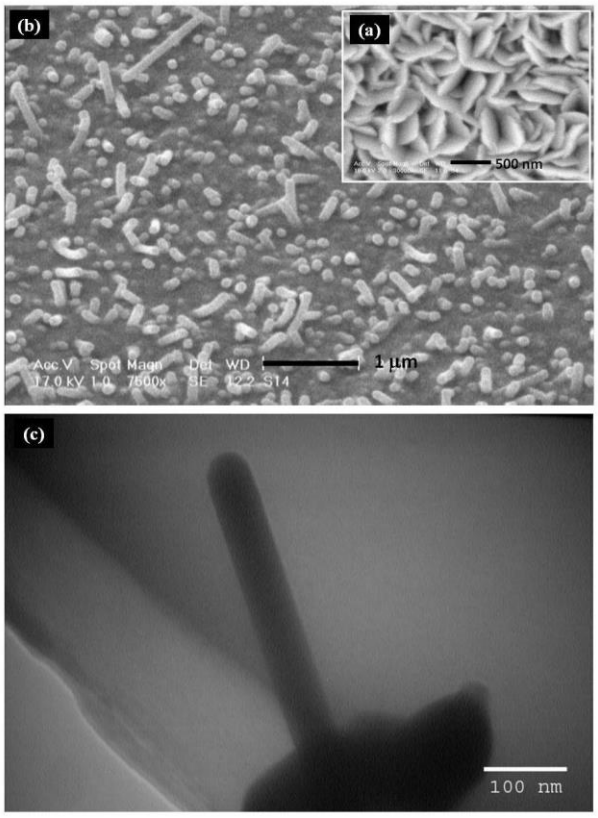

Fig. 4. FESEM images of sample B. (a) indicates the surface image of sample B before the first oxidation step and (b) shows the surface image of sample B after the second annealing process in oxygen flow. Scale bars for (a) and (b) images are 500 nm and 1 µm, respectively. (c) Indicates a TEM image of a single nanorod of sample B. The diameter of this nanorod is about 60 nm. Scale bar for TEM image is 100 nm.

The stronger (101) diffraction peak indicates that (101) is the preferred growth direction. It can be seen that the excess of oxygen flow in the second oxidation step has caused the structures to become more oxidized than in sample C and the higher temperature of the first oxidation step for sample B has resulted in a better crystalline structure. Of course the annealing time in oxygen for sample B had a substantial effect

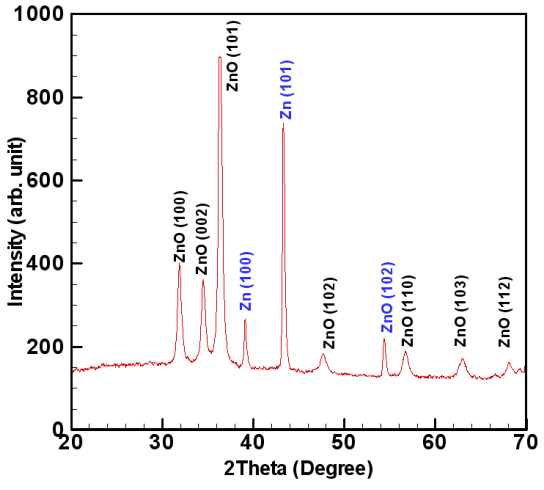

Fig. 5. The XRD pattern of sample B.

in both oxidation and crystallization of nanostructures in sample B. The XRD patterns of B and C samples indicate that by this method we can create samples by polycrystalline structures and we can concluded that increasing temperature of annealing in annealing process is responsible for beneficial crystalline of samples.

Figure 6 (a) shows the FESEM image of sample D before the first oxidation step. Sample D was not heat treated in vacuum prior to oxidation process and as it is seen, the deposited Zn layer is not in the form of nanosequins. By comparing sample D with samples A, B, C it can be realized that formation of nanosequins was the result of vacuum heat treatment. Figure 6 (b) indicates the surface image of sample D after the second oxidation step.

It is seen that the surface is covered with nanorods mostly with cone like ends. The distribution of the nanorods on the surface of sample D is not as uniform as sample B which is probably due to two parameters; first, not being heat treated in vacuum condition and, second, the lower pressure of annealing in the first oxidation step which for sample D was 1/5 of sample B.

To determine the optical properties of the grown ZnO nanorods photoluminescence measurement were performed at room temperature using a Xe lamp with an excitation wavelength of 300 nm. Figure 7 illustrates the PL spectra of sample B and D. Three bands were observed in the PL spectra of the ZnO nanorods. For sample D, a relatively broad peak in the range of 450 to 570 nm is seen, with a maximum centered at 523 nm, which is related to the green band emission. The green emission is attributed to the deep-level emission caused by structural defects such as oxygen vacancies and interstitial Zinc atoms. The green band in sample B is not as broad as in sample D and, although, the maximum of green band is located at the same position for both samples, the intensity of the green emission in sample B is not more than two third of sample D. This is mostly because, compared with sample D, sample B had been in exposure of

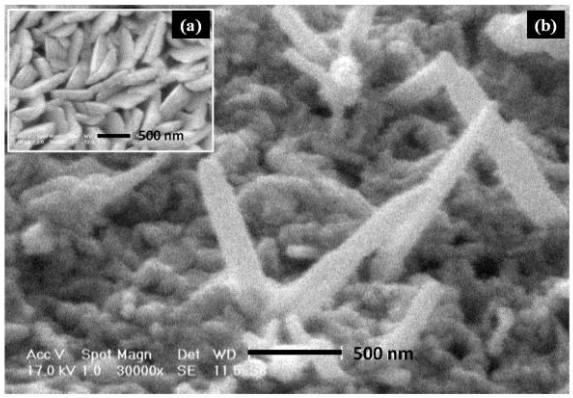

Fig. 6. (a) Shows the FESEM image of sample D before the first oxidation step, (b) indicates the surface image of sample D after the second oxidation step.

oxygen gas for a longer time and to a greater extent.

So, the number of oxygen vacancies was expected to be reduced. The second peak, which is centered at 440 nm for both samples, is related to the blue-violet emission.

The intensity of emission in this wavelength for sample B is almost twice of the sample D. The third peak centered at 390 nm, which is the strongest peak in the PL spectra, is related to the UV emission and it is known as near band edge emission (NBE). The greater intensity of UV emission in sample B relevant to sample D is probably because of its good crystallinity and indicates that the ZnO nanorods grown with this simple approach might be a proper kind of material for high- efficiency UV light emitting. Further work is ongoing to realize a rather pure UV emission.

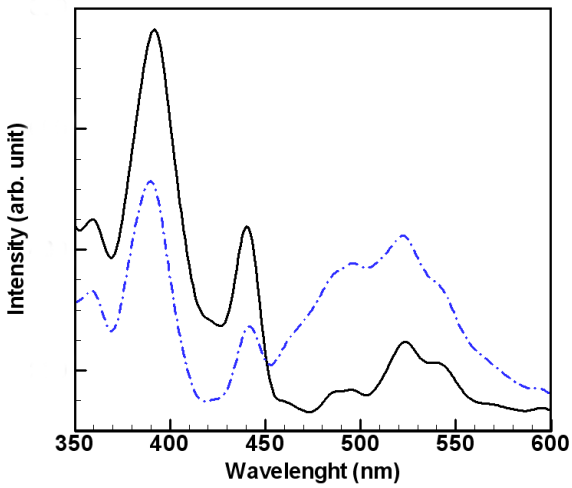

Fig. 7. Illustrates the PL spectra of sample B and D.

Generally three band have been observed in PL specrum for ZnO nanostructures: a UV peak attributed to near band edge emission of the wide band gap of ZnO, the blue-violet luminescence induced by radiation defects relevant to interface traps on grain boundary and produced from this level and valance level and the green emission is attributed to deep level emission caused by the impurities and structture defect such as zinc interstitials and oxygen vacancies. The green emission originates from the transition by the defect level of antisite oxide (O_{Zn}). The majority donors are oxygen vacancies (V_o) and zinc interstials (Z_{ni}).

The oxygen concentration related to Zn-O bonding increases; because of the increase in ZnO target sputtering power [18].

Antisite oxide (O_{Zn}) in the films at O-rich condition was easily formed from interstitial oxides (O_i) and zinc vacancies (V_{Zn}), because the antisite oxide has relatively low formation energy [19]. Vanheusden et al. [20], proved that the singly ionized oxygen vacancy is responsible for the green emission and this emission results from the recombination of a photogenerated hole with a singly ionized charge state of this defect.

4. Conclusions

Using metallic zinc granules and pure oxygen gas ZnO nanowires and nanorods with good crystallinity were synthesized by a simple evaporation method followed by a two-step oxidation process. Obtained nanowires and nanoroda are 70 and 100-150 nm in diameter respectively. X-ray pattern indicated the crystallinity and wurtzite structure of the products. The decrease of deep-level emission intensity in the PL spectra suggests that oxygen-related defects were reduced as a result of heat treatment in oxygen-rich atmosphere. The intensity of the near band emission was stronger than that of the deep-level emission, implying much improved crystal qualities. It is suggested that synthesis of ZnO nanorods and nanowires by the method employed in this experiment would be beneficial for fabricating ZnO nanostructures with good structural and optical properties to be used in UV optoelectronic devices.

References

1. S Choopun, R D Vispute, W Noch, A Balsamo, R P Sharma, T Venkatesan, A Iliadis and D C Look *Appl. Phys. Lett*. 75 (1999) pp. 3947.
2. Q Wan, H Li, Y J Chen, T H Wang, X L He, J P Li and C L Lin *Appl. Phys. Lett*. 84 (2004) pp. 3654.
3. D C Look *Mater. Sci. Eng*. B 80 (2001) pp. 383-387.
4. H Cao, J Y Xu, D Z Zhang, S H Chang, S T Ho, E W Seelig, X Liu and R P H Chang *Phys. Rev. Lett.* 84 (2000) pp. 5584-5587.
5. C Rath, S Singh, P Mallick, D Pandey, N P Lalla and N C Mishra *Indian J. Phys.* 83(4) (2009) pp. 415–421.
6. H Q Le, S J Chua, Y W Koh, K P Loh and E A Fitzgerald *J. Crys. Growth* 293 (2006) pp. 36–42.
7. J J Wu and S C Liu *Adv. Mater*. 14 (2002) pp. 215.
8. B P Zhang, N T Binh, Y Segawa, K Wakatsuki and N Usami *Appl. Phys. Lett*. 83 (2003) pp. 1635.
9. Z W Pan, Z R Dai and Z L Wang *Science* 291 (2001) pp. 1947.
10. J Y Lao, J Y Huang, D Z Wang, Z F Ren *Nano Lett*. 3 (2003) pp. 235.
11. R Chakraborty, U Das, D Mohanta and A Choudhury *Indian J. Phys*. 83(4) (2009) pp. 553-558.
12. S-W Kim, S Fujita and S Fujita *Appl. Phys. Lett.* 86 (2005) pp. 153119.
13. M H Huang, S Mao, H Feick, H Yan, Y Wu, H Kind, E Weber, R Russo and P Yang *Science*, 292 (2001) pp.1897-1899.
14. W I Park and G-C Yi *Adv. Mater*. 16 (2004) pp. 87-90.
15. F Krumeich, H J Muhr, M Niederberger, F Bieri, B Schnyder and R Nesper *J. Am. Chem. Soc*. 121, (1999) pp. 8324-8331.
16. J Q Hu, X L Ma, Z Y Xie, N B Wong, C S Lee and S T Lee *Chem. Phys. Lett*. 344 (2001) pp. 97.
17. B D Yao, Y F Chan and N *Wang Appl. Phys. Lett.* 81 (2002) pp. 757.
18. B J Jin, S Im and S Y Lee *Thin Solid Films*, 366 (2000) pp. 107.
19. E C Lee, Y S Kim, Y G Jin and K J Chang *Physica* B, 912(2001) pp. 308.
20. K Vanheusden, W L Warren, C H Seager, D R Tallant, J A Voigt and B E Gnade *J. Appl. Phys*, 79 (1996) pp. 7983.